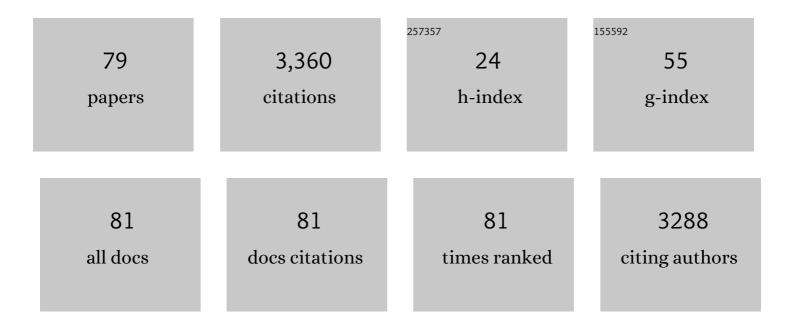
Jimin Wang

List of Publications by Year in descending order

Source: https://exaly.com/author-pdf/4552223/publications.pdf Version: 2024-02-01



LIMIN WANC

#	Article	IF	CITATIONS
1	Structure of a monomeric photosystem II core complex from a cyanobacterium acclimated to far-red light reveals the functions of chlorophylls d and f. Journal of Biological Chemistry, 2022, 298, 101424.	1.6	32
2	Structure of a photosystem I-ferredoxin complex from a marine cyanobacterium provides insights into far-red light photoacclimation. Journal of Biological Chemistry, 2022, 298, 101408.	1.6	16
3	High-resolution cryo-electron microscopy structure of photosystem II from the mesophilic cyanobacterium, <i>Synechocystis</i> sp. PCC 6803. Proceedings of the National Academy of Sciences of the United States of America, 2022, 119, .	3.3	58
4	Insights into Binding of Single-Stranded Viral RNA Template to the Replication–Transcription Complex of SARS-CoV-2 for the Priming Reaction from Molecular Dynamics Simulations. Biochemistry, 2022, 61, 424-432.	1.2	10
5	Two-Metal-Ion Catalysis: Inhibition of DNA Polymerase Activity by a Third Divalent Metal Ion. Frontiers in Molecular Biosciences, 2022, 9, 824794.	1.6	15
6	Glycerol binding at the narrow channel of photosystem II stabilizes the low-spin S2 state of the oxygen-evolving complex. Photosynthesis Research, 2022, , 1.	1.6	1
7	Structural Basis for Reduced Dynamics of Three Engineered HNH Endonuclease Lys-to-Ala Mutants for the Clustered Regularly Interspaced Short Palindromic Repeat (CRISPR)-Associated 9 (CRISPR/Cas9) Enzyme. Biochemistry, 2022, 61, 785-794.	1.2	12
8	Quantitative assessment of chlorophyll types in cryo-EM maps of photosystem I acclimated to far-red light. BBA Advances, 2021, 1, 100019.	0.7	6
9	RNA stabilization by a poly(A) tail 3′-end binding pocket and other modes of poly(A)-RNA interaction. Science, 2021, 371, .	6.0	29
10	Structural analyses of an RNA stability element interacting with poly(A). Proceedings of the National Academy of Sciences of the United States of America, 2021, 118, .	3.3	13
11	Identification of Mg ²⁺ ions next to nucleotides in cryo-EM maps using electrostatic potential maps. Acta Crystallographica Section D: Structural Biology, 2021, 77, 534-539.	1.1	9
12	Mechanism of Inhibition of the Reproduction of SARS-CoV-2 and <i>Ebola</i> Viruses by Remdesivir. Biochemistry, 2021, 60, 1869-1875.	1.2	12
13	Do crystallographic XFEL data support binding of a water molecule to the oxygen-evolving complex of photosystem II exposed to two flashes of light?. Proceedings of the National Academy of Sciences of the United States of America, 2021, 118, .	3.3	11
14	Computational insights into the membrane fusion mechanism of SARS-CoV-2 at the cellular level. Computational and Structural Biotechnology Journal, 2021, 19, 5019-5028.	1.9	10
15	Heterogeneous Composition of Oxygen-Evolving Complexes in Crystal Structures of Dark-Adapted Photosystem II. Biochemistry, 2021, 60, 3374-3384.	1.2	8
16	Structure of New Binary and Ternary DNA Polymerase Complexes From Bacteriophage RB69. Frontiers in Molecular Biosciences, 2021, 8, 704813.	1.6	3
17	Opportunities and challenges for assigning cofactors in cryo-EM density maps of chlorophyll-containing proteins. Communications Biology, 2020, 3, 408.	2.0	21
18	Crystal structure of the C-terminal domain of DENR. Computational and Structural Biotechnology Journal, 2020, 18, 696-704.	1.9	3

#	Article	IF	CITATIONS
19	Identification of a Na ⁺ -Binding Site near the Oxygen-Evolving Complex of Spinach Photosystem II. Biochemistry, 2020, 59, 2823-2831.	1.2	5
20	Visualization of H atoms in the Xâ€ray crystal structure of photoactive yellow protein: Does it contain Iowâ€barrier hydrogen bonds?. Protein Science, 2019, 28, 1966-1972.	3.1	6
21	Crystallographic identification of spontaneous oxidation intermediates and products of protein sulfhydryl groups. Protein Science, 2019, 28, 472-477.	3.1	13
22	Crystallographic evidence for twoâ€metalâ€ion catalysis in human pol Î∙. Protein Science, 2019, 28, 439-447.	3.1	13
23	Structure of HIV-1 reverse transcriptase cleaving RNA in an RNA/DNA hybrid. Proceedings of the National Academy of Sciences of the United States of America, 2018, 115, 507-512.	3.3	39
24	Determination of chemical identity and occupancy from experimental density maps. Protein Science, 2018, 27, 411-420.	3.1	11
25	Structural insights into the oligomerization of FtsH periplasmic domain from Thermotoga maritima. Biochemical and Biophysical Research Communications, 2018, 495, 1201-1207.	1.0	2
26	Structural and biochemical insights into inhibition of human primase by citrate. Biochemical and Biophysical Research Communications, 2018, 507, 383-388.	1.0	4
27	Misreading chaperone–substrate complexes from random noise. Nature Structural and Molecular Biology, 2018, 25, 989-990.	3.6	7
28	On the damage done to the structure of the <i>Thermoplasma acidophilum</i> proteasome by electron radiation. Protein Science, 2018, 27, 2051-2061.	3.1	5
29	Reduced Occupancy of the Oxygen-Evolving Complex of Photosystem II Detected in Cryo-Electron Microscopy Maps. Biochemistry, 2018, 57, 5925-5929.	1.2	3
30	Identification of ions in experimental electrostatic potential maps. IUCrJ, 2018, 5, 375-381.	1.0	22
31	Insights into Photosystem II from Isomorphous Difference Fourier Maps of Femtosecond X-ray Diffraction Data and Quantum Mechanics/Molecular Mechanics Structural Models. ACS Energy Letters, 2017, 2, 397-407.	8.8	16
32	On the appearance of carboxylates in electrostatic potential maps. Protein Science, 2017, 26, 396-402.	3.1	24
33	Systematic analysis of residual density suggests that a major limitation in wellâ€refined Xâ€ray structures of proteins is the omission of ordered solvent. Protein Science, 2017, 26, 1012-1023.	3.1	8
34	Experimental charge density from electron microscopic maps. Protein Science, 2017, 26, 1619-1626.	3.1	23
35	Effects of aligned αâ€helix peptide dipoles on experimental electrostatic potentials. Protein Science, 2017, 26, 1692-1697.	3.1	7
36	On contribution of known atomic partial charges of protein backbone in electrostatic potential density maps. Protein Science, 2017, 26, 1098-1104.	3.1	17

#	Article	IF	CITATIONS
37	On the relationship between cumulative correlation coefficients and the quality of crystallographic data sets. Protein Science, 2017, 26, 2410-2416.	3.1	7
38	Crystallographic Data Support the Carousel Mechanism of Water Supply to the Oxygen-Evolving Complex of Photosystem II. ACS Energy Letters, 2017, 2, 2299-2306.	8.8	58
39	Chlorophyll a with a farnesyl tail in thermophilic cyanobacteria. Photosynthesis Research, 2017, 134, 175-182.	1.6	12
40	On the interpretation of electron microscopic maps of biological macromolecules. Protein Science, 2017, 26, 122-129.	3.1	47
41	Xâ€ray radiationâ€induced addition of oxygen atoms to protein residues. Protein Science, 2016, 25, 1407-1419.	3.1	17
42	Destructionâ€andâ€diffraction by Xâ€ray freeâ€electron laser. Protein Science, 2016, 25, 1585-1592.	3.1	5
43	Oxygen additions in serial femtosecond crystallographic protein structures. Protein Science, 2016, 25, 1797-1802.	3.1	12
44	S ₃ State of the O ₂ -Evolving Complex of Photosystem II: Insights from QM/MM, EXAFS, and Femtosecond X-ray Diffraction. Biochemistry, 2016, 55, 981-984.	1.2	62
45	Estimation of the quality of refined protein crystal structures. Protein Science, 2015, 24, 661-669.	3.1	19
46	On the validation of crystallographic symmetry and the quality of structures. Protein Science, 2015, 24, 621-632.	3.1	9
47	Comment on "Crystal structures of translocator protein (TSPO) and mutant mimic of a human polymorphism― Science, 2015, 350, 519-519.	6.0	5
48	Diamonds in the rough: a strong case for the inclusion of weak-intensity X-ray diffraction data. Acta Crystallographica Section D: Biological Crystallography, 2014, 70, 1491-1497.	2.5	17
49	Exploiting subtle structural differences in heavy-atom derivatives for experimental phasing. Acta Crystallographica Section D: Biological Crystallography, 2014, 70, 1873-1883.	2.5	3
50	Structural models of the membrane anchors of envelope glycoproteins E1 and E2 from pestiviruses. Virology, 2014, 454-455, 93-101.	1.1	10
51	Structural Changes in the Oxygen-Evolving Complex of PhotosystemÂll Induced by the S ₁ to S ₂ Transition: A Combined XRD and QM/MM Study. Biochemistry, 2014, 53, 6860-6862.	1.2	46
52	Structural insights into the stabilization of MALAT1 noncoding RNA by a bipartite triple helix. Nature Structural and Molecular Biology, 2014, 21, 633-640.	3.6	213
53	Exploiting large non-isomorphous differences for phase determination of a G-segment invertase–DNA complex. Acta Crystallographica Section D: Biological Crystallography, 2014, 70, 685-693.	2.5	4
54	Calcium-dependent conformational transition of calmodulin determined by Fourier transform infrared spectroscopy. International Journal of Biological Macromolecules, 2013, 56, 57-61.	3.6	6

#	Article	IF	CITATIONS
55	Crystal structure of an intermediate of rotating dimers within the synaptic tetramer of the G-segment invertase. Nucleic Acids Research, 2013, 41, 2673-2682.	6.5	24
56	Crystal structure of glycoprotein E2 from bovine viral diarrhea virus. Proceedings of the National Academy of Sciences of the United States of America, 2013, 110, 6805-6810.	3.3	108
57	Structural and mechanistic insights into guanylylation of RNA-splicing ligase RtcB joining RNA between 3′-terminal phosphate and 5′-OH. Proceedings of the National Academy of Sciences of the United States of America, 2012, 109, 15235-15240.	3.3	53
58	Using a Fluorescent Cytosine Analogue tC ^o To Probe the Effect of the Y567 to Ala Substitution on the Preinsertion Steps of dNMP Incorporation by RB69 DNA Polymerase. Biochemistry, 2012, 51, 4609-4617.	1.2	7
59	Structural Basis for Differential Insertion Kinetics of dNMPs Opposite a Difluorotoluene Nucleotide Residue. Biochemistry, 2012, 51, 1476-1485.	1.2	10
60	Bidentate and tridentate metalâ€ion coordination states within ternary complexes of RB69 DNA polymerase. Protein Science, 2012, 21, 447-451.	3.1	8
61	Probing Minor Groove Hydrogen Bonding Interactions between RB69 DNA Polymerase and DNA. Biochemistry, 2012, 51, 4343-4353.	1.2	17
62	Structural Insights into Complete Metal Ion Coordination from Ternary Complexes of B Family RB69 DNA Polymerase. Biochemistry, 2011, 50, 9114-9124.	1.2	35
63	Insights into Base Selectivity from the 1.8 Ã Resolution Structure of an RB69 DNA Polymerase Ternary Complex. Biochemistry, 2011, 50, 581-590.	1.2	43
64	Variation in Mutation Rates Caused by RB69pol Fidelity Mutants Can Be Rationalized on the Basis of Their Kinetic Behavior and Crystal Structures. Journal of Molecular Biology, 2011, 406, 558-570.	2.0	18
65	Tertiary architecture of the <i>Oceanobacillus iheyensis</i> group II intron. Rna, 2010, 16, 57-69.	1.6	68
66	Inclusion of weak high-resolution X-ray data for improvement of a group II intron structure. Acta Crystallographica Section D: Biological Crystallography, 2010, 66, 988-1000.	2.5	25
67	Poly(A) Tail Recognition by a Viral RNA Element Through Assembly of a Triple Helix. Science, 2010, 330, 1244-1247.	6.0	144
68	RB69 DNA Polymerase Mutants with Expanded Nascent Base-Pair-Binding Pockets Are Highly Efficient but Have Reduced Base Selectivity. Biochemistry, 2009, 48, 6940-6950.	1.2	24
69	Hoogsteen base-pairing in DNA replication?. Nature, 2005, 437, E6-E7.	13.7	29
70	A Twisted Four-Sheeted Model for an Amyloid Fibril. Structure, 2005, 13, 1279-1288.	1.6	27
71	Correction of X-ray intensities from single crystals containing lattice-translocation defects. Acta Crystallographica Section D: Biological Crystallography, 2005, 61, 67-74.	2.5	38
72	Correction of X-ray intensities from an HslV–HslU co-crystal containing lattice-translocation defects. Acta Crystallographica Section D: Biological Crystallography, 2005, 61, 932-941.	2.5	22

#	Article	IF	CITATIONS
73	Crystal structure of a self-splicing group I intron with both exons. Nature, 2004, 430, 45-50.	13.7	431
74	Visualizing a Circadian Clock Protein. Molecular Cell, 2004, 15, 375-388.	4.5	179
75	A Corrected Quaternary Arrangement of the Peptidase HslV and ATPase HslU in a Cocrystal Structure. Journal of Structural Biology, 2001, 134, 15-24.	1.3	23
76	Structure of the Replicating Complex of a Pol \hat{I}_{\pm} Family DNA Polymerase. Cell, 2001, 105, 657-667.	13.5	547
77	Crystal Structure Determination ofEscherichia coliClpP Starting from an EM-Derived Mask. Journal of Structural Biology, 1998, 124, 151-163.	1.3	46
78	The 2.4 à crystal structure of the bacterial chaperonin GroEL complexed with ATPγS. Nature Structural Biology, 1996, 3, 170-177.	9.7	243
79	X-ray structures of recombinant yeast cytochrome c peroxidase and three heme-cleft mutants prepared by site-directed mutagenesis. Biochemistry, 1990, 29, 7160-7173.	1.2	145